AEM JOURNAL.ORG

Temperature-Control Technology for Optical Communication Modules Based on Micro-Thermoelectric Cooler

Bin Zheng
Tianjin Institute of Power Sources, The 18th Research Institute of China Electronics Technology Group Corporation, Tianjin 300384, China
Corresponding author: Bin Zheng (e-mail: zhengbin_cetc18@163.com)

ABSTRACT Micro-thermoelectric cooler (Micro-TEC) is a semiconductor thermoelectric conversion device based on the Peltier effect and can provide localized temperature control for temperature-sensitive devices. With the rapid development of electronic information industries and the increasing integration density of semiconductor devices, key parameters of optical communication modules have become highly sensitive to temperature variations, directly influencing optical and electromagnetic signal transmission quality. This work proposes an active temperature-control technology for optical communication modules based on Micro-TEC. Design parameters are derived from the thermoelectric cooling model, and high-strength Bi_2Te_3-based thermoelectric materials are prepared by hot extrusion. The thermoelectric performance of hot-extruded Bi_2Te_3 is improved through halogen-compound doping and solid-solution composition regulation. By integrating surface treatment, particle fabrication, assembly integration, and overall soldering processes, a practical fabrication method for Micro-TEC is developed. At 300 K, the measured maximum temperature difference reaches 69.53 K, and the Bi_2Te_3 particle integration density exceeds 1000 particles/cm^2. Application verification in an optical module confirms effective photonic-chip temperature control, showing potential in communications, lasers, infrared systems, optics, and electromagnetic signal-stability applications.

INDEX TERMS micro-TEC, thermoelectric cooling, Bi_2Te_3, optical communication module, electromagnetic signal stability

I. INTRODUCTION

Thermoelectric cooler (TEC) is fabricated from semiconductor materials based on the Peltier effect [1,2]. TEC can rapidly transfer heat and offer several advantages, including small size, low weight, noise-free operation, long service life, absence of moving parts, and maintenance-free operation. By changing the current direction, TEC can also provide heating, making them suitable for localized and precise point-specific temperature control. In recent years, with the rapid development of 5G communication, artificial intelligence, optical detection, advanced sensing, autonomous driving, and related fields, the integration level of semiconductor devices has increased substantially. Core devices such as chips, lasers, and sensors are characterized by extremely small volumes and highly concentrated heat generation. Using TEC for precise temperature control of these devices is an effective approach to solving their thermal management problems [3–5].

This issue is particularly important in the field of optical communications. Photonic chips, as the core components of optical communication modules, are highly sensitive to temperature variations. Key parameters such as wavelength, output power, sensitivity, and reliability are strongly affected by temperature fluctuations, directly influencing signal transmission quality and stability. With the rapid development of next-generation communication technology and the accelerated deployment of AI clusters and data centers, the market demand for high-speed optical transceiver modules has increased rapidly. Temperature control has consequently become a technical bottleneck restricting the development of the optical communication industry. Active temperature-control technology based on TEC is a feasible solution for thermal management in optical communication modules. However, optical modules are extremely small, generate concentrated heat, and are installed in very limited space. Therefore, Micro-TEC is required for temperature control, with stringent requirements imposed on both cooling capacity and power consumption [6–8]. At present, relevant research groups have conducted studies on thermodynamic structural design [9,10], numerical simulation [11,12], and thermoelectric material preparation [13]. However, there are still relatively few reports on the fabrication of Micro-TEC and the application verification of Micro-TEC active temperature control technology. The technical support for industrial application is still insufficient.

In this work, an active temperature control technology based on Micro-TEC is proposed. Micro-TEC with miniaturized and highly integrated features are used to control the temperature of core devices with small volumes and concentrated heat generation. Micro-TEC design and simulation were performed, Micro-TEC samples were fabricated, and performance testing and application verification were carried out. The verification results show that the Micro-TEC can meet the temperature control requirements of optical modules. Micro-TEC also can be further extended to heat dissipation and temperature control scenarios involving various devices with extremely small volumes, concentrated heat generation, and limited installation space.

II. MICRO-TEC DESIGN SCHEME

A. WORKING PRINCIPLE AND BASIC PARAMETERS OF TEC

A TEC consists of multiple P and N type thermoelectric particle pairs connected electrically in series, the thermoelectric micro-pillars (elements) have rectangular cross sections. Pure copper interconnects are used as electrodes, and the P and N type thermoelectric particles are connected by soldering to form a complete electrical circuit. The cold and hot sides are coupled to the external environment through alumina or aluminum nitride ceramic plates. A schematic structure of TEC is shown in Fig. 1(a), and the energy conversion principle of TEC is shown in Fig. 1(b). The main performance parameters of TEC include the maximum temperature difference $\Delta T_{\max}$, voltage at maximum temperature difference $V_{\max}$, current at maximum temperature difference $I_{\max}$, maximum cooling power $Q_{C\max}$, resistance R, and dimensionless figure of merit zT.

Dimensionless figure of merit zT: Also referred to as the thermoelectric figure of merit, zT is expressed as Eq. (2-1).

$$zT = \frac{\alpha^2 \sigma T}{\kappa} \tag{2-1}$$

As indicated by the above equation, the thermoelectric figure of merit zT is determined comprehensively by the Seebeck coefficient, electrical conductivity, and thermal conductivity of the thermoelectric materials. A higher zT value corresponds to higher thermoelectric conversion efficiency, greater maximum cooling power, higher maximum temperature difference, and improved cooling performance of the TEC.

Maximum temperature difference $\Delta T_{\max}$: This parameter refers to the maximum achievable temperature difference between the hot side and cold side when the TEC operates with zero heat load and the hot side temperature is fixed at a specified value. The unit is K or °C.

Current at maximum temperature difference $I_{\max}$: This parameter refers to the operating current required for the TEC to achieve the maximum temperature difference. The unit is A.

Under the maximum temperature difference operating mode, the current at maximum temperature difference is given by Eq. (2-2),

$$I_{\max} = \frac{(\alpha_P - \alpha_N)}{R} T_C \tag{2-2}$$

where T_C is the cold side temperature.

Maximum cooling power $Q_{C\max}$: This parameter refers to the cooling power when the TEC operates at $I_{\max}$, and the temperature difference is 0 K. The unit is W.

Under thermal equilibrium, the maximum cooling power of a cooling module composed of n thermoelectric couple pairs is expressed as Eq. (2-3),

$$Q_{C\max} = n(\alpha T_C I_{\max} - 0.5 I_{\max}^2 R - K\Delta T) \tag{2-3}$$

where R and K is given by Eq. (2-4).

$$\begin{aligned} R &= \frac{l_N}{A_N}\rho_N + \frac{l_P}{A_P}\rho_P, \\ K &= \frac{A_N}{l_N}\kappa_N + \frac{A_P}{l_P}\kappa_P \end{aligned} \tag{2-4}$$

The first term in Eq. (2-3) represents the Peltier heat, the product of the Seebeck coefficient and the cold side temperature is the Peltier coefficient at the cold junction of the thermoelectric couple. The second term represents half of the Joule heat, assuming that half of the Joule heat generated in the thermoelectric couple during operation is transferred to the cold junction. The third term represents the heat conducted from the hot junction to the cold junction according to Fourier's law of heat conduction. However, as the dimensions of the thermoelectric micro-pillars are reduced to the 0.2 mm scale, the "size effect" and interfacial thermal resistance between the Bi_2Te_3 materials and the copper electrodes become significant. To maintain the accuracy of the Micro-TEC theoretical model, an effective thermal conductivity K_{eff} is introduced, which incorporates the contact thermal resistance at the heterogeneous interfaces, ensuring the model remains valid at the micro-scale.

Voltage at maximum temperature difference $V_{\max}$: This parameter refers to the voltage of the TEC when it operates at $I_{\max}$. The unit is V.

Under the maximum temperature difference operating mode, the voltage drop generated across one P–N pair is expressed as Eq. (2-5),

$$v_{\max} = I_{\max} r + (\alpha_P - \alpha_N)\Delta T \tag{2-5}$$

with $\alpha = \alpha_P - \alpha_N$, Eq. (2-6) can be obtained,

$$v_{\max} = \frac{\alpha T_C}{r} r + \alpha(T_H - T_C) = \alpha T_H \tag{2-6}$$

where T_H is the hot side temperature. For a TEC with n thermoelectric couple pairs, the voltage at maximum temperature difference is expressed as Eq. (2-7).

$$V_{\max} = n v_{\max} \tag{2-7}$$

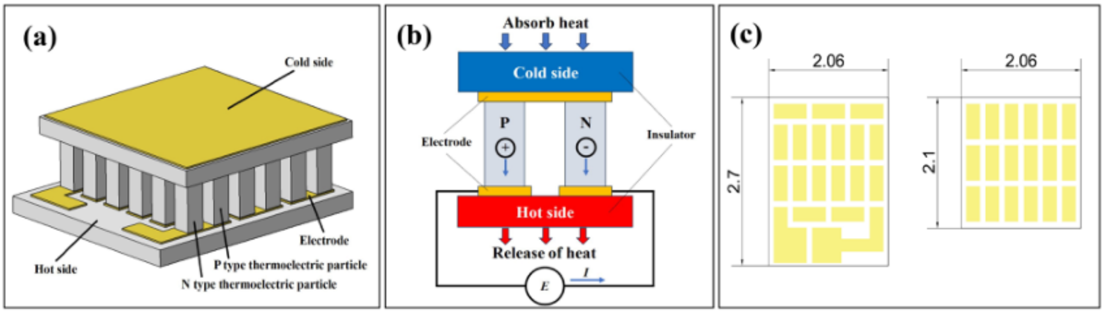

FIGURE 1. (a) Schematic structure of TEC; (b) Schematic diagram of the energy conversion principle of TEC; (c) Schematic of the Micro-TEC ceramic circuit.

Resistance R: This parameter refers to the total resistance of all thermoelectric couple pairs in the TEC. The unit is Ω.

The resistance of one thermoelectric couple pair composed of one P type and one N type thermoelectric particle is given by Eq. (2-8),

$$r = \frac{l_N}{\sigma_N s_N} + \frac{l_P}{\sigma_P s_P} \quad (2\text{-}8)$$

where l_N and l_P are the lengths of the P and N type thermoelectric particles, respectively, and s_N and s_P are their cross-sectional areas, respectively. The resistance of a TEC with n thermoelectric couple pairs is expressed as Eq. (2-9).

$$R = nr \quad (2\text{-}9)$$

From the above definitions, it can be concluded that when a TEC reaches its maximum temperature difference, its cooling power is zero; when it reaches its maximum cooling power, the temperature difference is zero.

B. THERMOELECTRIC PERFORMANCE AND STRUCTURAL DESIGN OF TEC

The Seebeck coefficient ranges of Bi_2Te_3 rods are as follows: $|\alpha_N| \geq (210 \pm 10)$ μV/K; $|\alpha_P| \geq (210 \pm 10)$ μV/K. The electrical conductivity ranges are as follows: $\sigma_N = (1000 \pm 100)$ $\Omega^{-1}\cdot$cm^{-1}; $\sigma_P = (1100 \pm 100)$ $\Omega^{-1}\cdot$cm^{-1}. According to the application requirements of optical communication modules, Micro-TEC design was carried out by taking photonic chips used in 100G, 200G, and 400G optical modules for optical communications and data centers as examples. In terms of thermoelectric parameter design, the heat generation power of a photonic chip is approximately 0.3 W. When the TEC hot side temperature is 358 K (85 °C), the photonic chip temperature, corresponding to the TEC cold side temperature, must be maintained below 318 K (45 °C). In other words, a temperature difference exceeding 40 K must be generated under a 0.3 W heat load. Meanwhile, under this operating condition, the TEC power consumption must not exceed 2.5 W. In addition, according to the power supply requirements, the maximum operating voltage at room temperature is limited to 2.1 V. In the context of high-density data centers, the Power Usage Effectiveness (PUE) of the optical module is a critical metric. Therefore, the design of the Micro-TEC prioritizes low power consumption. By optimizing the geometry of the thermoelectric couples and minimizing internal resistance, the Micro-TEC maintains the chip temperature with a power budget that accounts for less than 15% of the total module power, ensuring that the active cooling technology enhances reliability without compromising the overall energy efficiency of the system. In terms of external dimensions, the installation space for the TEC is extremely limited, the Micro-TEC size is restricted to 2.7 × 2.06 × 0.85 mm in length × width × height.

Based on the above conditions and the thermoelectric parameter calculation expressions for TEC, Eqs. (2-2)–(2-8), the voltage drop per thermoelectric couple pair under the maximum temperature difference operating mode can be calculated as Eq. (2-10).

$$v_{\max} = I_{\max} r + \alpha \Delta T_{\max} = \frac{\alpha T_C}{r} + \alpha (T_H - T_C) = \alpha T_H \quad (2\text{-}10)$$

According to the design requirements, the maximum operating voltage at room temperature is 2.1 V. Assuming the hot side temperature T_H = 300 K (27 °C), and taking $V_{\max}$ = 2.1 V as the voltage at maximum temperature difference of TEC, the number of TEC thermoelectric couple pairs can be calculated from Eqs. (2-9) and (2-10). After integer rounding, the number of thermoelectric couple pairs is determined to be 18.

Based on the operating conditions of optical communication modules, the following parameters were used: hot side temperature T_H = 358 K (85 °C), cold side temperature T_C = 318 K (45 °C), and cooling power Q_C = 0.25 W. According to the characteristics of Bi_2Te_3 materials, the Seebeck coefficients were selected as $\alpha_N = -210$ μV/K and $\alpha_P = 210$ μV/K, the electrical conductivities were selected as $\sigma_N = 1000$ $\Omega^{-1}\cdot$cm^{-1} and $\sigma_P = 1100$ $\Omega^{-1}\cdot$cm^{-1}, and the thermal conductivities were selected as $\kappa_N = 1.4$ W/(m·K) and $\kappa_P = 1.4$ W/(m·K). By substituting the above parameters into Eqs. (2-5)–(2-7), the thermoelectric design parameters of the TEC were obtained. During the calculation of the relevant thermoelectric parameters, the processing difficulty associated with TEC assembly, integration, and soldering was also considered. In general, the spacing between Bi_2Te_3 particles should be greater than 0.1 mm. Based on the above considerations, the basic dimensional parameters of the Micro-TEC were determined as follows.

The Bi_2Te_3 micro-pillar size was selected as 0.2 × 0.2 × 0.3 mm in length × width × height. The particles were arranged in a rectangular array with a spacing of 0.12 mm. A total of 18 N–P thermoelectric couple pairs were included. The envelope area of the N–P thermoelectric couple pairs was 2.1 × 2.06 mm. On the hot side of the Micro-TEC, pads for wire bonding were reserved. A schematic of the Micro-TEC ceramic circuit is shown in Fig. 1(c). Based on the above parameters and the actual operating requirements, when the hot side temperature T_H is 300 K (27 °C), the maximum cooling power $Q_{C\max}$ of the Micro-TEC can reach 1.0 W. Under ideal conditions, for a 0.3 W heat load and a power consumption of 2.0 W, the cold side temperature T_C can reach 303 K (30 °C), satisfying the operating requirements for temperature control of the photonic chips. Meanwhile, considering the effects of thermal resistance, heat leakage, and other factors in practical applications, a considerable design margin was incorporated.

The ceramic substrate is an important raw material for Micro-TEC and serves two main functions. First, it provides mechanical structural support and connects the module to the temperature-controlled object and heat sink, thereby forming a heat transfer path. Second, the copper electrodes on its surface form an electrical conduction path together with the P and N type thermoelectric couple pairs. A high-thermal-conductivity aluminum nitride ceramic substrate was selected for the Micro-TEC, and the copper electrodes were fabricated using a direct plated copper (DPC) process [14,15]. Compared with conventional alumina substrates, the high-thermal-conductivity aluminum nitride substrate has lower thermal resistance and higher heat transfer efficiency, which is more favorable for rapidly dissipating heat from photonic chips in confined spaces. In addition, the DPC process uses sputter deposition to prepare a seed layer on the substrate surface, followed by electroplating and photolithography to form the circuit, compared with the traditional DBC and AMB substrates, the DPC process enables smaller dimensions, narrower spacing, and higher-precision integration of electrodes [16]. The ceramic substrate thickness of the Micro-TEC was 0.2 mm, the spacing between electrodes was 0.1 mm, and the copper layer thickness of the electrodes was 20–30 μm, which meets the requirement for carrying a current of 1 A.

III. FABRICATION OF MICRO-TEC

A. PREPARATION OF Bi_2Te_3 THERMOELECTRIC MATERIALS

The P and N type Bi_2Te_3 particles that constitute the thermoelectric couple pairs are the key components determining TEC performance. Bi_2Te_3 materials exhibit a high Seebeck coefficient, high electrical conductivity, and low thermal conductivity, their optimal operating temperature range is from room temperature to 473 K (200 °C), making Bi_2Te_3 the best room temperature thermoelectric materials for semiconductor cooling. For Micro-TEC fabrication, thermoelectric materials must possess both high thermoelectric performance to satisfy the maximum temperature difference requirement and high mechanical strength to enable the fabrication of small particles. Bi_2Te_3 materials prepared by the conventional zone-melting technique have insufficient mechanical strength. Therefore, in this work, high performance and high strength Bi_2Te_3 materials were prepared by hot extrusion. Hot extrusion, also known as hot plastic forming, is a process in which materials are heated to a temperature above the recrystallization temperature and then extruded through diameter reduction [17]. A schematic of the hot extrusion die and hot extrusion principle is shown in Fig. 2(a).

In this work, Bi_2Te_3 hot extrusion precursors were prepared by high-frequency melting, followed by hot extrusion to produce material rods. The core part of the extrusion chamber was funnel-shaped, with an inlet diameter of 100 mm and an outlet diameter of 30 mm. The hot extrusion temperature was 500–550 °C, and the extrusion rate was less than 1 mm/s. The compression ratio of more than 3:1, combined with an extrusion rate below 1 mm/s, facilitates directional arrangement of crystal grains. Bi_2Te_3 material rods prepared by hot extrusion are shown in Fig. 2(b). The prepared Φ30 mm hot extruded P and N type Bi_2Te_3 rods exhibited bending strengths of 55–60 MPa and compressive strengths of 183–204 MPa. The mechanical strength was approximately three times higher than that of materials prepared by the conventional zone-melting technique. The materials showed good formability, smooth surfaces, and no cracks. Arrayed particles prepared from hot extruded Bi_2Te_3 materials are shown in Fig. 2(c), and a single particle observed by scanning electron microscopy (SEM) is shown in Fig. 2(d). The high strength Bi_2Te_3 material rods enabled the fabrication of particles with minimum dimensions of 0.2 × 0.2 × 0.2 mm, satisfying the Micro-TEC requirement for small particle fabrication.

Micro-TEC requires materials that not only satisfy high mechanical strength requirements but also exhibit excellent thermoelectric performance. For N-type Bi_2Te_3 materials, $Bi_2Te_{2.79}Se_{0.21}$ was selected as the matrix, and TeI_4 was used as the dopant to regulate the electron concentration [18,19]. Figure 2(e) shows the temperature dependence of the thermoelectric figure of merit zT for $Bi_2Te_{2.79}Se_{0.21}$ + x wt% TeI_4. For $Bi_2Te_{2.79}Se_{0.21}$ without TeI_4 doping, the zT value decreases continuously over the entire measured temperature range because the carrier concentration is relatively low and the material approaches intrinsic conduction. After TeI_4 doping, the zT value first increases and then decreases with increasing temperature. When the TeI_4 doping content is 0.1 wt%, the zT value reaches its maximum of 0.92.

For P-type Bi_2Te_3 materials, Te was selected as the dopant, and the composition of the Bi_2Te_3-Sb_2Te_3 solid solution was adjusted to improve the thermoelectric performance [20,21]. Figure 2(f) shows the temperature dependence of zT for $(Bi_2Te_3)_x(Sb_2Te_3)_{1-x}$ + 3 wt% Te. With increasing Bi_2Te_3 content, the peak zT gradually shifts toward the low temperature region, which is more favorable for cooling applications near room temperature. When the material composition is $Bi_{0.5}Sb_{1.5}Te_3$ + 3 wt% Te, the zT value reaches its maximum of 1.07. In summary, the hot extrusion process primarily enhanced the mechanical strength and grain orientation, while halogen compound doping and solid solution composition regulation were responsible for optimizing the carrier concentration. Control experiments using traditional zone-melted materials with identical doping levels indicated that the synergistic effect of hot extrusion and precise doping led to a 15% higher zT compared to doping alone, ensuring excellent thermoelectric performance that reaches a leading level among commercial Bi_2Te_3 materials.

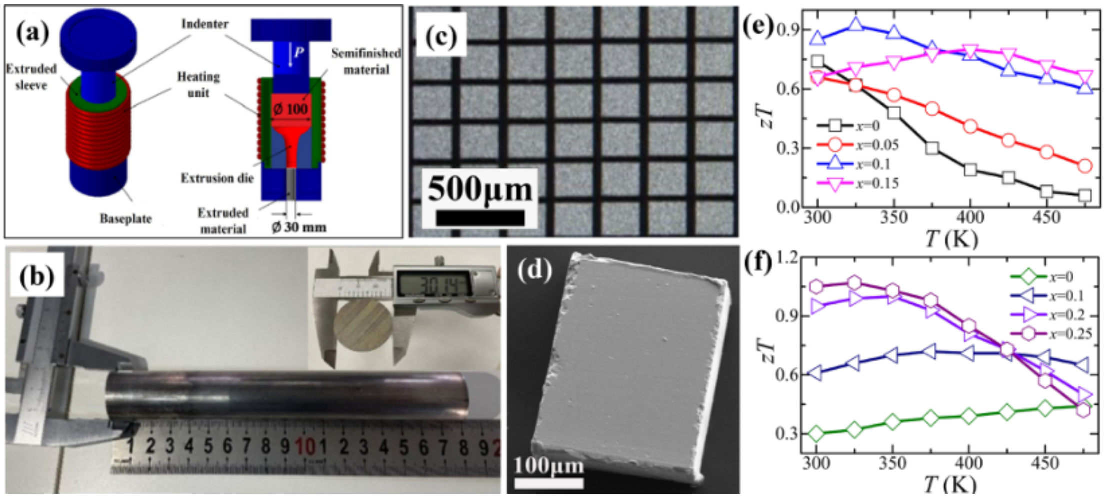

FIGURE 2. (a) Schematic of the hot extrusion die and hot extrusion principle; (b) Bi_2Te_3 material rod prepared by hot extrusion; (c) Arrayed particles prepared from high strength Bi_2Te_3 material rods; (d) SEM image of a single miniature Bi_2Te_3 particle; (e) Temperature dependence of the thermoelectric figure of merit zT for N-type $Bi_2Te_{2.79}Se_{0.21}$ + x wt% TeI_4 materials, where $x = 0$, 0.05, 0.1, and 0.15; (f) Temperature dependence of the thermoelectric figure of merit zT for P-type $(Bi_2Te_3)_x(Sb_2Te_3)_{1-x}$ + 3 wt% Te materials, where $x = 0$, 0.1, 0.2, and 0.25.

B. ASSEMBLY OF MICRO-TEC

A feasible method for assembling Micro-TEC was developed in this work. The specific steps are as follows:

1) Bi_2Te_3 material rods were cut into material slices with a thickness of 0.3 mm by wire cutting.
2) The surfaces of the material slices were treated by degreasing with a metal cleaning agent, ultrasonic cleaning, and roughening with a roughening solution consisting of concentrated sulfuric acid and concentrated nitric acid, in order to obtain surfaces suitable for plating.
3) An 8–10 μm thick nickel layer was prepared by electroplating or chemical plating as a diffusion barrier layer, and a 5–8 μm thick tin layer was deposited to improve the solderability of the material slices.
4) The material slices were diced by internal circular slicing to produce particles with fixed dimensions and to form an arrayed arrangement.
5) Tin paste with a thickness of 0.15 mm was uniformly coated on the copper electrodes of the ceramic substrate by screen printing.
6) Using surface-mount technology, the Bi_2Te_3 particles were picked up by a suction nozzle and mounted on the surface of the hot side ceramic substrate electrodes coated with tin paste.
7) A flip-chip bonder was used to complete alignment and soldering of the Micro-TEC. The flip-chip bonder can clearly observe the relative positions of the cold and hot side ceramic substrates through upper and lower light sources and cameras, and it is equipped with manual alignment, heating, and pressure functions. First, the heating function of the equipment was used to cure the Bi_2Te_3 particles on the hot side. Subsequently, the cured hot side Micro-TEC semi-finished product was picked up and aligned with the cold side ceramic substrate. After precise alignment and closure, simultaneous heating and pressure were applied to complete soldering of the Micro-TEC.
8) The finished Micro-TEC was cleaned to remove flux and other impurities.

Micro-TEC samples were fabricated using the above process. A Micro-TEC semi-finished product after particle mounting is shown in Fig. 3(a), and the finished Micro-TEC is shown in Figs. 3(b) and 3(c). The SEM characterization of the solder joints after sectioning is shown in Fig. 3(d). The integration density of Bi_2Te_3 particles in the Micro-TEC exceeded 1000 particles/cm^2 (in the Micro-TEC samples prepared in this work, the particle integration density reached 1230 particles/cm^2). Based on this fabrication process, various Micro-TECs can be prepared with Bi_2Te_3 particle sizes ranging from 0.2 × 0.2 × 0.2 mm to 1.0 × 1.0 × 1.0 mm, Bi_2Te_3 particle spacings ranging from 0.1 to 0.8 mm, and Micro-TEC dimensions ranging from 1.8 × 1.8 × 0.85 mm to 10.0 × 10.0 × 3.0 mm. These Micro-TEC products can be adapted to temperature control requirements of different types of chips and sensors, including optical communication modules, pump lasers, LiDAR systems, infrared imaging systems, optical sensors, and gas sensors.

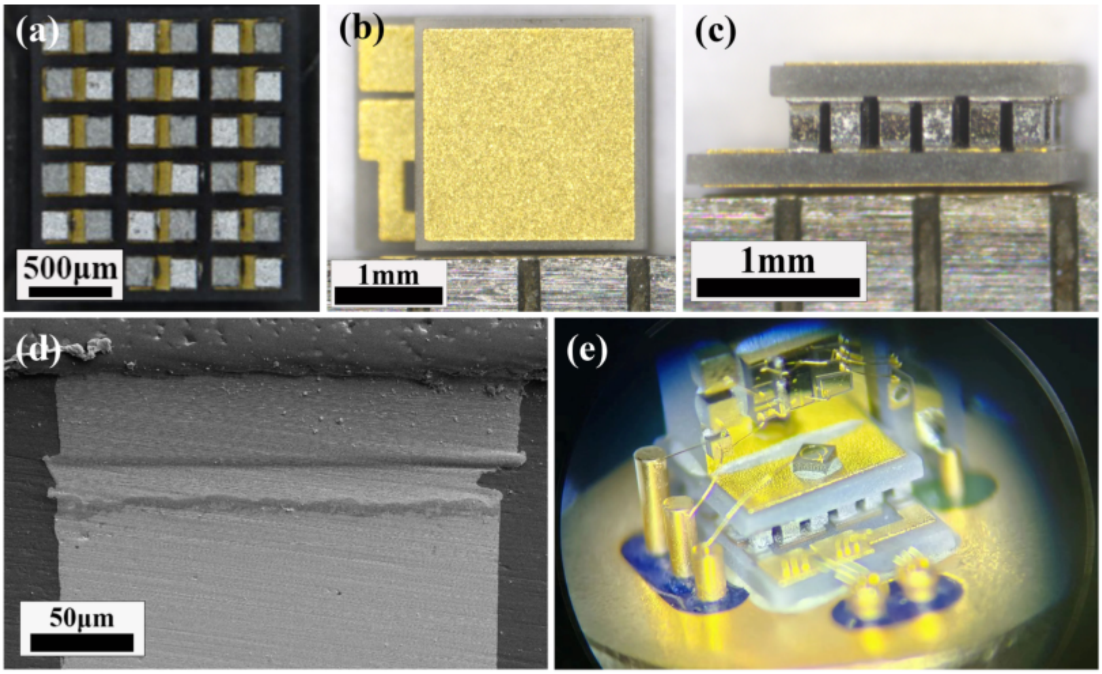

FIGURE 3. (a) Micro-TEC semi-finished product after particle mounting; (b) Finished Micro-TEC product, top view; (c) Finished Micro-TEC product, side view; (d) SEM characterization of solder joints after sectioning of the finished Micro-TEC product; (e) Installation of the Micro-TEC and photonic chip after packaging in an optical module.

IV. EXPERIMENTAL VERIFICATION OF MICRO-TEC

A. THERMOELECTRIC PERFORMANCE TESTING OF MICRO-TEC

The thermoelectric parameters of Micro-TEC were measured under vacuum conditions. During testing, the hot side of the Micro-TEC was tightly attached to a heat sink, which was connected to a water-circulation temperature control system below it. This system enabled precise control of the TEC hot side temperature. A heating resistor was placed in close contact with the cold side of the TEC, and the electrical power applied to the heating resistor was regarded as the heat load. Thermocouples were connected to both the cold and hot sides of the TEC to monitor the real-time temperatures. At a hot side temperature of $T_H = 300$ K (27 °C), with no heat load applied to the cold side, the temperature difference reached when the TEC operated at the $I_{\max}$, was defined as the maximum temperature difference $\Delta T_{\max}$. When the TEC operated at $I_{\max}$, the heat load was increased until the temperature difference between the cold and hot sides became 0 K, at this point, the applied heat load was defined as the maximum cooling power $Q_{C\max}$.

Five Micro-TEC samples were selected for testing. At a hot side temperature of $T_H = 300$ K (27 °C), the $\Delta T_{\max}$ of the samples ranged from 68.47 to 69.53 K, and the $Q_{C\max}$ of the samples ranged from 0.992 to 1.026 W. The $\Delta T_{\max}$ of the Micro-TEC samples were already very close to that of conventional TECs with standard dimensions [22–24]. Furthermore, the stability of the fabricated Micro-TEC was evaluated across the full industrial temperature range of 233 K to 358 K (-40 °C to 85 °C). The variation in the figure of merit (ZT) for both P and N-type materials remained

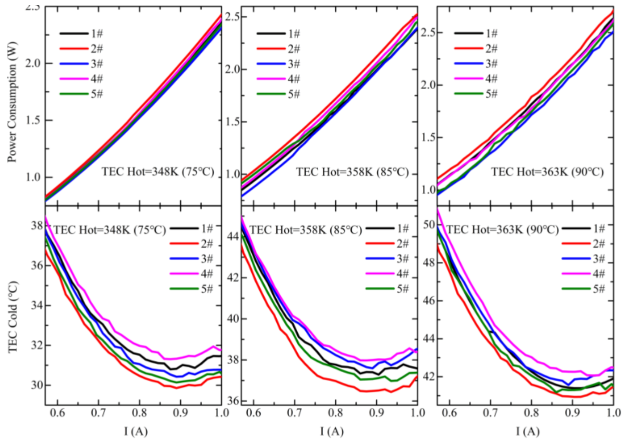

FIGURE 4. Temperature-control capability test results of the Micro-TEC packaged with a photonic chip in an optical module.

within $\pm 5\%$ across this range, confirming the robustness of the halogen-doped Bi_2Te_3 materials. Detailed testing results across these fluctuating environments demonstrate that the Micro-TEC can provide consistent temperature regulation for optical transceiver modules operating under extreme external conditions.

B. APPLICATION VERIFICATION OF MICRO-TEC

The Micro-TEC was packaged together with a photonic chip in an optical communication module, and the temperature-control capability of the Micro-TEC for the photonic chip was tested. The installation of the Micro-TEC and photonic chip after packaging in the optical module is shown in Fig. 3(e), and the test results are shown in Fig. 4.

When the TEC hot side temperature was $T_H = 358$ K (85 °C), applying a current of 0.6–1.0 A to the TEC enabled the photonic chip temperature to be controlled below 318 K (45 °C), with a minimum temperature of 309.5 K (36.5 °C), the power consumption of the Micro-TEC was below 2.5 W. When the TEC hot side temperature was $T_H = 363$ K (90 °C), applying a current of 0.75–0.9 A still enabled the photonic chip temperature to be controlled below 318 K (45 °C), and the power consumption below 2.5 W. The verification results indicate that, due to thermal resistance, environmental heat leakage, and other factors, the actual performance of the Micro-TEC was lower than the simulated design results. Nevertheless, the Micro-TEC satisfied the application requirement of maintaining the photonic chip temperature below 318 K (45 °C) at a TEC hot side temperature of 358 K (85 °C). To maintain this localized cooling effect and prevent thermal crosstalk in high-density environments, the hot side heat was efficiently exported through the high-thermal-conductivity AlN substrate to the module's external shell, which acts as a secondary heat sink. This integration ensures that the "specific point" temperature control does not lead to localized heat accumulation within the module housing.

V. CONCLUSIONS

In this work, the design, fabrication, and testing of Micro-TEC was investigated. According to the application requirements of optical modules, customized Micro-TEC products were designed. High strength and high performance Bi_2Te_3 thermoelectric materials were prepared by combining hot extrusion with material modification technologies, enabling the fabrication of Bi_2Te_3 particles at the 0.2 mm scale. The thermoelectric figure of merit zT reached 0.92 for N-type Bi_2Te_3 materials and 1.07 for P-type Bi_2Te_3 materials, representing a leading level among commercial Bi_2Te_3 materials.

Micro-TEC fabrication was completed through heterogeneous interface preparation, fabrication of miniature Bi_2Te_3 particles, high density assembly integration, and overall soldering. At a hot side temperature of 300 K (27 °C), the measured maximum temperature difference $\Delta T_{\max}$ of the Micro-TEC reached 69.53 K, and the integration density of Bi_2Te_3 particles exceeded 1000 particles/cm^2. Application verification was conducted using optical modules, and the results demonstrated that the Micro-TEC can meet the temperature-control requirements of optical communication modules. Moreover, Micro-TEC fabricated using the method described in this work can be extended to multiple fields, including communications, lasers, infrared systems, and optics, providing a useful reference for precise temperature-control solutions for core chips and devices in these fields.

AUTHOR CONTRIBUTIONS

Bin Zheng designed, collected and analyzed the data, and drafted the manuscript. Bin Zheng conducted the study, critically revised the manuscript for important intellectual content, and gave final approval of the version to be published. Bin Zheng participated fully in the work, take public responsibility for appropriate portions of the content, and agreed to be accountable for all aspects of the work in ensuring that questions related to the accuracy or integrity of any part of the work are appropriately investigated and resolved.

CONFLICTS OF INTEREST

The authors declare no conflict of interest.

FUNDING

This research received no external funding.

ACKNOWLEDGEMENTS

Not applicable.

REFERENCES

[1] D. M. Rowe, Thermoelectrics Handbook: Macro to Nano. Boca Raton: CRC/Taylor & Francis, 2005.

[2] J. Mao, G. Chen, and Z. Ren, "Thermoelectric cooling materials," Nature Materials, 2020, doi: 10.1038/s41563-020-00852-w.

[3] B. C. Sales, "Smaller is cooler," Science, vol. 295, no. 5558, pp. 1248–1249, 2002, doi: 10.1126/science.1069895.

[4] R. Chein and G. Huang, "Thermoelectric cooler application in electronic cooling," Applied Thermal Engineering, vol. 24, no. 14–15, pp. 2207–2217, 2004, doi: 10.1016/j.applthermaleng.2004.03.001.
[5] J. He and T. M. Tritt, "Advances in thermoelectric materials research: looking back and moving forward," Science, vol. 357, no. 6358, eaak9997, 2017, doi: 10.1126/science.aak9997.
[6] A. Majumdar, "Thermoelectric devices: helping chips to keep their cool," Nature Nanotechnology, vol. 4, no. 4, p. 214, 2009, doi: 10.1038/nnano.2009.65.
[7] Q. Zhang, K. Deng, L. Wilkens, et al., "Micro-thermoelectric devices," Nature Electronics, vol. 5, pp. 333–347, 2022, doi: 10.1038/s41928-022-00776-0.
[8] K. M. Shilpa, M. A. Raheman, A. Aabid, et al., "A systematic review of thermoelectric peltier devices: applications and limitations," 2023, 19(1):20, doi: 10.32604/fdmp.2022.020351.
[9] Y. Liu, D. Yang, K. Tang, et al., "Enhanced design optimization of microthermoelectric cooler in optical module," Solid State Sciences, vol. 160, 2025, doi: 10.1016/j.solidstatesciences.2025.107829.
[10] Y. Lei, X. Du, Y. Wei, et al., "Hotspot thermal management using thermoelectric and microchannel hybrid cooling at transient and steady states," Applied Thermal Engineering, vol. 265, 2025, doi: 10.1016/j.applthermaleng.2025.125556.
[11] T. Gong, C. Ma, L. Cao, et al., "On-chip hotspot thermal delay and peak clipping using a heterogeneously integrated micro-thermoelectric cooler," Applied Thermal Engineering, vol. 278, Part B, 2025, doi: 10.1016/j.applthermaleng.2025.127258.
[12] X. Chen, H. Xia, J. Feng, et al., "Theoretical and numerical study on the impact of intrinsic properties, interfacial contacts, and direct current coupling in thermoelectric transient cooling for hotspot elimination under alternating current mode," Materials Today Physics, 101744, 2025, doi: 10.1016/j.mtphys.2025.101744.
[13] C. Lin, X. Ma, K. Liang, et al., "Miniaturized Mg_3Bi_2-based thermoelectric cooler for localized electronic thermal management," Nature Communications, vol. 16, 7779, 2025, doi: 10.1038/s41467-025-63174-y.
[14] Wei, "Direct plated copper substrate for RF and microwave packaging applications," in Proc. IEEE, 2010, doi: 10.1109/IMPACT.2010.5699546.
[15] H. Ru, V. Wei, T. Jiang, et al., "Direct plated copper technology for high brightness LED packaging," in Proc. IEEE, 2011, doi: 10.1109/IMPACT.2011.6117219.
[16] Q. Sun, Y. Peng, H. Cheng, et al., "Direct ink writing of 3D cavities for direct plated copper ceramic substrates with kaolin suspensions," Ceramics International, vol. 45, no. 9, p. 9, 2019, doi: 10.1016/j.ceramint.2019.03.191.
[17] Q. Zhang, K. Pang, Y. Wu, et al., "Robust $Bi_2(Te,Se)_3$ thermoelectrics from large shrinkage ratio extrusion drives advanced peltier microcooler and power generator," Advanced Functional Materials, 2500731, 2025, doi: 10.1002/adfm.202500731.
[18] Z. Tang, L. Hu, T. Zhu, et al., "High performance n-type bismuth telluride based alloys for mid-temperature power generation," Journal of Materials Chemistry C, vol. 3, 2015, doi: 10.1039/C5TC02263K.
[19] L. Hu, T. Zhu, X. Liu, et al., "Point defect engineering of high-performance bismuth-telluride-based thermoelectric materials," Advanced Functional Materials, 1400474, 2014, doi: 10.1002/adfm.201400474.
[20] M. Wang, Q. Zhang, Y. Wu, et al., "Constructing multiple microstructures in Sb_2Te_3-based thermoelectrics enables a high-performance segmented power generator," Journal of Materials Chemistry A: Materials for Energy and Sustainability, vol. 13, no. 26, 2025, doi: 10.1039/D5TA02986D.
[21] J. R. Sootsman, D. Y. Chung, and M. G. Kanatzidis, "New and old concepts in thermoelectric materials," Angewandte Chemie International Edition, vol. 48, pp. 8616–8639, 2009.
[22] B. Qin, D. Wang, X. Liu, et al., "Power generation and thermoelectric cooling enabled by momentum and energy multiband alignments," Science, vol. 373, no. 6554, pp. 556–561, 2021, doi: 10.1126/science.abi8668.
[23] S. Wang, Y. Wen, S. Bai, et al., "Realizing high-performance thermoelectric modules through enhancing the power factor via optimizing the carrier mobility in n-type PbSe crystals," Energy & Environmental Science, vol. 17, no. 7, pp. 2588–2597, 2024, doi: 10.1039/d4ee00433g.
[24] J. Liu, F. Liu, Y. Li, et al., "High-performance near-room-temperature n-type Bi_2Te_3-based thermoelectric alloys with superior mechanical properties," Science China Materials, vol. 68, no. 3, 2025, doi: 10.1007/s40843-024-3058-7.